ARTICLES

Hydrated Cs+-Exchanged MFI Zeolites: Location of Extraframework Species in $Cs_xH_yMFI \cdot zH_2O$ Phases from X-ray Powder Diffraction and Differential Molar Adsorption Calorimetry

Bernard F. Mentzen*

RZHGC, 5 rue Marcel Desplaces, F-69330 Meyzieu, France

Gairat U. Rakhmatkariev

Institute of General and Inorganic Chemistry, Academy of Scienes of Uzbekistan, 77a Kh. Abdullaev Ave., UZ-700170 Tashkent, Uzbekistan

Gérard Bergeret

IRCELYON (Institut de Recherches sur la Catalyse et l'Environnement de Lyon), UMR 5256 CNRS-Université Lyon 1, 2 avenue Albert-Einstein, F-69626 Villeurbanne, France

Hans-Peter Weber

ACCE , Grand Vivier, F-38960 France

Received: November 20, 2006; In Final Form: January 10, 2007

The locations and populations of extraframework species in zeolitic Cs-exchanged H−MFI materials have recently been reported both in several fully dehydrated phases (*J. Phys. Chem. B* **2006,** *110,* 97−106) and in hydrated $Cs_{6.6}H_{0.3}MFI \cdot zH_2O$ (1.5 < z < 28) samples (*J. Phys. Chem. B* **2006,** *110,* 13741−13752). The present paper extends our study to more general compositions, i.e., $Cs_xH_yMFI \cdot zH_2O$ phases spanning the range 0.7 < x < 7.7, 0.3 < y < 5.3 and 4 < z < 32. Structural information is obtained from Rietveld refinements of laboratory X-ray powder diffraction data collected at room temperature (RT, 22 or 26 °C). We discovered that flushing fully hydrated $Cs_xH_yMFI \cdot zH_2O$ samples with a stream of dinitrogen (N_2) gas corresponds to a rather strong isothermal water desorption effect. This effect is intimately correlated with the origin (synthesis method, postsynthesis treatments, and defect concentration) of the Cs-exchanged sample. Special attention is focused on the $Cs_{2.3}H_{1.1}MFI \cdot 24H_2O$ sample, for which high precision differential molar adsorption calorimetry data corresponding to its complete hydration process exist. In order to be able to interpret the observed water adsorption heats, we had to take several correlations into account: those existing between the Si/Al ratio and the (H,Li,Na,Cs)/uc cationic contents versus water loadings, in addition to the specific interactions between the cations or protons with aromatics as benzene or *p*-xylene. It is shown that in the 0−4.5 Al/uc range the maximum water/uc content, in all of the investigated H−MFI samples, is strictly proportional to the Al/uc values (about 8.5 water molecules per Al/uc). In most cation exchanged samples, this value is significantly different: it is either lower (e.g., Na and Cs) or higher (e.g., Li). In the case of *p*-xylene sorbed in fully dehydrated H−MFI materials (0 < H/uc < 4.5), all samples adsorb about eight molecules/uc, whereas the presence of extraframework cations lowers dramatically this sorption capacity. It is shown that the crystallinity of a ZSM-5 zeolite might be conveniently estimated by simply inspecting the XRPD profile corresponding to the *p*-xylene saturated parent H−MFI phase. In this work, it is shown how calorimetric data can be exploited to complement crystal structure results and detect subtle sorbent/sorbate interactions on the molecular level, which cannot be revealed by Rietveld-type powder diffraction profile structure refinements alone. The influence of structural defects (essentially −OH silanol groups attached to Si/Al framework atoms) on the observed adsorption heats is particularly pronounced. The host/guest interactions, observed at very low water loadings for the $Cs_{2.3}H_{1.1}MFI$/water system, are estimated by computer simulations (molecular mechanics (MM) calculations).

Hydrated Cs$^+$-Exchanged MFI Zeolites

J. Phys. Chem. C, Vol. 111, No. 10, 2007 **3821**

1. Introduction

MFI-type zeolitic crystalline solids (silicalite, ZSM-5 and postsynthesis modified phases) are probably one of the most widely investigated microporous synthetic materials.[1] These materials belong to the pentasil zeolites group. Their framework structure is built up from 5−1 secondary building units (SBU). The pore system of this zeolite type consists of medium sized cavities, also known as channel intersections (sites I), which are interconnected through zigzag (also called sinusoidal) channel sections (ZZ, sites II) by 10-ring pore openings in the [100] axis direction and straight channel sections (SC, sites III) by 10-ring pore openings in the [010] axis direction. The labeling of sites I, II, and III corresponds to the chronological characterization by single crystal or powder X-ray diffraction structure refinements of extraframework guest molecules in low-aluminum containing MFI solids (genuine silicalites with Si/Al > 150). For sites I and II, the best structure determinations correspond to the silicalite·**4**TPA[2] (tetrapropylammonium structure directing template molecule located at the channel intersection) and silicalite·**8**p-xylene[3] (in ref 3 the XYL2 species is located in the zigzag channel section) complexes, respectively. For site III, the first unambiguous crystal structure determination corresponds to the silicalite·**8**benzene complex[4,5] (one benzene species in site I and the second one in site III). The 10-ring pore openings in the MFI channel system range from almost circular (nonbonded framework O···O distances = 8.45 × 7.92 Å)[2] to highly elliptical (O···O distances = 9.23 × 7.07 Å) in a silicalite·**8**p-nitroaniline complex.[6] These 10-ring sections are also described in terms of kinetic diameter openings; in that case, the O···O distances must be corrected for the van der Waals interaction distance of the oxygen atom, its commonly accepted value being 1.40 Å. In that case, the above-mentioned pore openings are 5.65 × 5.12 Å for the circular section and 6.43 × 4.27 Å for the elliptical one, respectively.

The MFI type framework is rather flexible. This flexibility is the direct consequence of specific host/guest interactions between the bare MFI framework and the extraframework species. For instance, in the ZSM-5·4tripropylbenzylammonium as-synthesized complex,[7] the benzyl group located in the straight channel section (site III) causes an elliptical 10-ring pore opening deformation, since its kinetic diameter (6.0 ± 0.2 Å) is significantly greater than that of a circular section (mean section ∼5.4 Å). The flexibility of the MFI 10-ring channel pore openings has recently also been observed in the case of Cs-exchanged ZSM-5 materials presenting Si/Al ratios and Cs/unit-cell (uc) concentrations in the 10−70 and 0.7−7.7 ranges, respectively.[8,9] Except for the lowest Cs/uc containing phase (0.7 Cs/uc), all of the dehydrated[8] and hydrated[9] CsMFI type materials display strongly elliptical straight channel 10-ring pore opening deformations. It appears that the Cs cation, in its isolated or hydrated states, is the actual driving force for this unique effect. If this effect is easily conceivable for the hydrated phases, where the Cs2 (see ref 9) occurs as bulky hydrogen-bonded Cs$_2$(H$_2$O)$_5$ type clusters which run through the straight channel sections (shortest Cs1-Ow1 = 2.86, Cs2-Ow1 = 2.86, and Cs3-Ow2 = 2.82 Å distances, ref 9), it is less so in the case of isolated Cs cations, which are loosely bonded to the O(fr) framework oxygen atoms (shortest Cs2−O11 = 3.33 and Cs3'-O25 = 3.08 Å distances, ref 8). Nevertheless, in the latter case, it has to be interpreted in terms of specific short-range ionic interactions between the positively charged Cs cation(s) and the charge-balancing negative charges distributed on a limited number of framework oxygen atoms close to Al/Si substitution centers.

The present work is a continuation of our studies on the same dehydrated and hydrated zeolitic CsMFI/water host/guest systems.[8,9] In the case of fully dehydrated Cs$_x$MFI phases, we have shown that for the 0.7 < Cs/uc < 7.7 cation concentration range at room temperature (28 °C), as well as at higher temperatures (up to 450 °C), linear correlations exist between the individual Cs1/uc, (Cs2 + Cs2')/uc and (Cs3 + Cs3')/uc concentrations and the total Cs/uc formula content. These correlations prove that in the Cs$_x$MFI phases the incorporation mechanism of the cation is unique and does not depend on the origin or the Cs/uc value of the Cs-exchanged sample. We now extend our investigations to the hydrated phases corresponding to several Cs$_x$H$_y$MFI·zH$_2$O compositions, viz 0.7 < x < 7.7, 0.3 < y < 5.3, and 4 < z < 32. In our last paper we have established that in the hydrated Cs$_{6.6}$MFI·nH$_2$O phases (1.5 < n < 28) only three distinct Cs species are characterized and localized.[9] In the present paper, we focus our attention on the Cs$_{2.3}$H$_{1.1}$MFI·24H$_2$O sample, for which high precision differential molar adsorption calorimetry data corresponding to its complete hydration process have been measured (33 isothermal equilibrium points at 30 °C). To be able to interpret the structural details obtained by the combined use of X-ray powder diffractometry and adsorption calorimetry, correlations had to be developed between the Si/Al ratio and the (H,Li,Na,Cs)/uc cationic contents versus water loadings. Some specific interactions observed between the cation or the proton and sorbed aromatics (benzene, p-xylene) must also be developed. The crystal structure results corresponding to fully and partially hydrated Cs$_x$H$_y$MFI·zH$_2$O (after 6 h of flushing in a dry N$_2$ gas stream at 26 °C − isothermal desorption) are compared and discussed.

2. Experimental Section

The starting Cs$_x$H$_y$MFI·zH$_2$O materials are fully described in ref 8. The experimental X-ray powder diffraction data are collected at the IRCELYON (Institut de Recherches sur la Catalyse et l'Environnement de Lyon, Villeurbanne, France), using a Panalytical X'Pert Pro MPD diffractometer (Cu Kα radiation, Panalytical X'Celerator detector). The samples are mounted on the temperature-regulated stainless steel sample-holder (flat reflection geometry) in a controlled atmosphere (dry N$_2$ flow) Anton Paar XRK 900 reactor chamber. In each case, three in situ X-ray powder diffraction patterns (XRPD) are recorded for each sample: the first one corresponds to the room temperature (26 °C) water saturated phase after 6 h of flushing with dry N$_2$, the second one corresponds to the anhydrous sample dehydrated at 450 °C (already reported in ref 8), and the third one corresponds to the anhydrous sample at room temperature (also reported in ref 8). The XRPD patterns corresponding to the fully hydrated phases are obtained in separate ex situ experiments. The recorded patterns are corrected for instrumental parameters and all the structure refinements are performed by using the Rietveld method (with a locally modified version of the DBW3.2[10] code and the EXPGUI version of GSAS[11]).

The high precision differential molar adsorption calorimetry is performed on a Tian-Calvet derived calorimeter at the Institute of General and Inorganic Chemistry (Tashkent, Uzbekistan). A complete description of this device is given elsewhere.[12] About 0.2 g of the fully hydrated Cs$_{2.3}$H$_{1.1}$MFI·24H$_2$O zeolite is compacted into small pellets and subsequently crushed. The resulting tiny zeolitic grains (about 0.5 × 0.5 × 0.5 mm^3) are placed in the calorimeter sample holder in a shallow-bed

* Corresponding author. E-mail: mentzen.b@infonie.fr.

TABLE 1: Unit-Cell Parameters (in Å) for the Water Saturated Cs_xMFI Materials at 22 °C

Cs/uc	H/uc	a	b	c	α(°)	uc/V (Å³)	water/uc	ε
0.7	0.7	20.0919(6)	19.8969(7)	13.3890(6)	90.308(4)[a]	5352.5(5)	16(1)[b]	1.060[c]
1.6	2.2	20.075(1)	19.911(1)	13.4004(9)		5356(1)	24(1)	1.078
2.0	1.6	20.0513(7)	19.9053(7)	13.3899(6)		5344.2(5)	19(1)	1.121
2.1	2.5	20.1623(8)	19.9481(8)	13.4399(7)		5405.5(6)	29(1)	1.058
2.3	**1.1**	**20.0928(8)**	**19.9045(8)**	**13.3934(4)**		**5356.5(5)**	**25(1)**	**1.149**[e]
2.9	5.3	20.0586(7)	19.9243(7)	13.4095(6)		5366.4(5)	21(2)	1.156
3.2	5.0	20.0677(6)	19.9312(6)	13.4128(5)		5364.8(4)	20(1)	1.154
3.5	1.1	20.0789(6)	19.9297(6)	13.4109(5)		5366.0(6)	32(2)	1.140
4.0	4.8	20.0611(8)	19.9121(8)	13.3907(7)		5349.0(6)	32(1)	1.179
5.4	3.4	20.058(1)	19.923(1)	13.397(1)		5354(1)	32(1)	1.146
6.6	0.3	20.0592(2)	19.9411(2)	13.4300(2)[d]		5372.0(2)	28(1)	1.164
7.7	1.1	20.078(1)	19.929(1)	13.407(1)		5364.6(9)	**31**(1)	1.146

[a] This phase is monoclinic with $P2_1/n11$ framework symmetry (α deformation angle as reported in ref 8). [b] Verified by adsorption isotherms at 22 °C. [c,d] See refs 8 and 9. [e] See section 3.3.

configuration and carefully heated up to 500 °C under high vacuum and maintained at that temperature for an additional 10 h. After complete cooling down to ambient temperature (30 °C), the adsorption isotherm and the differential adsorption heats are measured simultaneously. A usual high precision calorimetry run concerns 40–60 individual experimental points, corresponding each to an isothermal (usually at 30 °C) equilibrium at a given pressure and sorbate loading. So many equilibrium points are usually not considered when investigating a sorbent/sorbate system by diffraction techniques. Additional calorimetric curves corresponding to the silicalite/benzene and the silicalite/*p*-xylene systems are also described and interpreted.

The computer simulation method used to estimate the adsorption heats at lower water loadings (in the case of the $Cs_{2.3}H_{1.1}$MFI/H_2O system) is of the nonbonded atom–atom van der Waals interaction type. Methodology and values for the exp-6–1 nonbonding potential parameters are reported in refs 8 and 9. Experimental water adsorption capacities are obtained by thermogravimetric heating/cooling cycles.

3. Results from Diffraction Experiments

3.1. Structures of the Fully Hydrated Phases (RT 22 °C). To determine the evolution of the locations and populations of the exchanged Cs cations and water molecules in the Cs_xH_y-MFI·zH_2O phases, the XRPD patterns recorded ex situ (12 hydrated phases) are analyzed by the Rietveld structure refinement method. The unit-cell parameters and straight channel ellipticities (ε) are reported in Table 1. Given that all these phases correspond to fully hydrated samples, it is not surprising that their main structural features (three Cs species, six water species, their relative populations and locations) are comparable to those already detailed and reported for the $Cs_{6.6}H_{0.3}$MFI· 28H_2O phase in ref 9. Therefore only a few particularly relevant structural parameters are available as Supporting Information (Tables 1S–4S). It must be emphasized that, within experimental errors, all of the refined water saturation loadings in the fully hydrated phases are close to multiples of 4. This observation is a direct consequence of the MFI channel system, which presents four channel intersection (sites I), four zigzag channel sections (sites II) and four straight channel sections (sites III) per unit-cell. In Figure 1, the evolutions of the individual Cs1/uc, Cs2/uc, and Cs/3 populations versus total Cs/uc concentrations (Figure 1b) are compared to the same type of correlations observed in the case of the fully dehydrated Cs_xMFI phases (Figure 1a). These figures clearly show that the incorporation mechanism of the three distinct Cs1, Cs2, and Cs3 species in the Cs_xMFI phases obeys linear correlations versus total Cs/uc
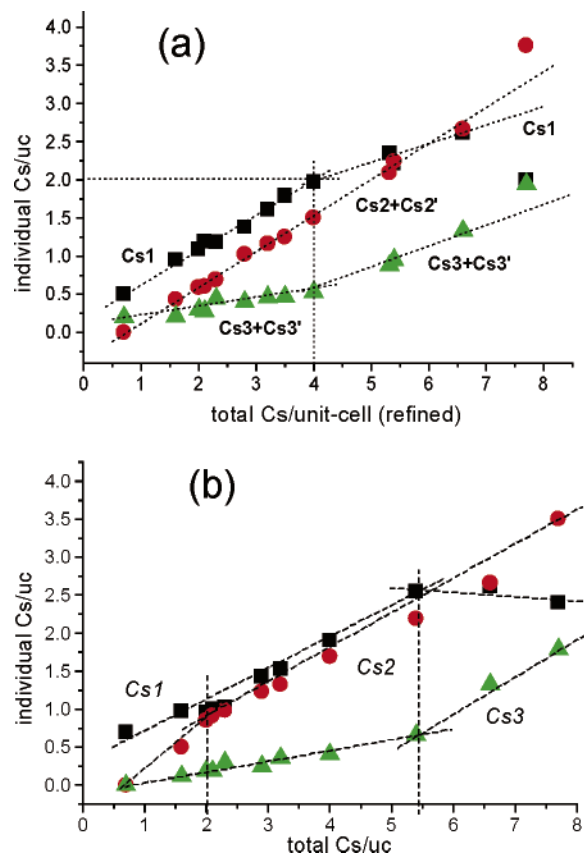

Figure 1. Evolution of the individual Cs1/uc (squares), Cs2/uc + Cs2′/ uc or Cs2/uc (circles), and Cs3/uc + Cs3′/uc or Cs3/uc (triangles) populations vs total Cs/uc content at room temperature: (a) in the dehydrated and (b) in the fully hydrated Cs_xH_yMFI·zH_2O phases.

for both the dehydrated and the fully hydrated phases. In ref 9, it is shown that a Cs cation occupies the space of about 2.3–3 water molecules in the zeolitic MFI channel system, and that the theoretical maximum water/uc in a totally cation free MFI amounts to 48 molecules/uc. The highest Cs-exchanged MFI phase corresponds to the $Cs_{7.7}H_{1.1}$MFI·31H_2O one, and its estimated maximum water/uc filling should be about 24.9 to 30.3 (48−Cs/uc × 3 or Cs/uc × 2.3). The refined 31(1) water/ uc loading (Table 1) is close to one of the estimated maximum values and is therefore considered as acceptable. The crystal structure of the $Cs_{2.3}H_{1.1}$MFI·24H_2O phase is detailed in section 3.3.

3.2. Structures of the Hydrated Phases Flushed under N₂ Gas Flow (RT 26 °C). Table 2 reports the results for eight samples flushed with dry N₂ (the partial dehydration equilibrium,

Hydrated Cs$^+$-Exchanged MFI Zeolites

J. Phys. Chem. C, Vol. 111, No. 10, 2007 **3823**

TABLE 2: Unit-Cell Parameters (in Å) for Some N$_2$ Flushed Cs$_x$MFI Materials at 26 °C

Cs/uc	H/uc	a	b	c	α(°)	uc/V (Å^3)	water/uc	ε
0.7	0.7	20.0743(7)	19.8872(8)	13.3797(6)	90.286(2)^a	5341.5(5)	15(1)	1.065^b
1.6	2.2	20.0659(6)	19.9092(6)	13.3940(5)		5350.8(5)	4.5(8)	1.146
2.0	1.6	20.0459(6)	19.9056(6)	13.3861(5)		5341.4(5)	7(1)	1.163
2.1	2.5	20.0854(5)	19.9307(5)	13.4060(4)		5366.6(6)	12(1)	1.149
2.3	**1.1**	**20.0784(7)**	**19.9061(7)**	**13.3888(6)**		**5351.3(5)**	**8.4(4)**	**1.108**
2.9	5.3	20.0435(5)	19.9183(5)	13.3993(4)		5349.4(5)	6.5(6)	1.192
3.5	1.1	20.0748(6)	19.9263(6)	13.4082(5)		5363.5(4)	21(2)	1.134
5.4	3.4	20.039(1)	19.910(1)	13.3807(9)		5339(1)	9(1)	1.213

^{a} See Table 1. ^{b} For the straight channel ellipticity (ε) definition see refs 8 and 9. ε corresponds to the ratio between the longest and the shortest O···O distances in the 10-rings of the MFI framework structure.

checked by monitoring the diffracted intensity of the intense peak close to 8° (2θ), is reached after ~6 h of N$_2$ flushing at 26 °C. The crystal structure parameter tables corresponding to some of these zeolitic phases are available as Supporting Information (Tables 5S−8S). The isothermal water desorption effect caused by a dry He or N$_2$ flushing gas-stream on fully hydrated zeolitic materials (LTA, FAU, ERI, MOR, MFI)[1] at room temperature is a commonly observed phenomenon.[13−15] In some instances, this dehydration can represent a substantial part of the total water loading. If we compare the water/uc loadings in Tables 1 and 2, it appears that the observed minimum/maximum isothermal desorption percentages are 6 and 81%, respectively. Apparently there is no obvious correlation between the chemical composition and the isothermal water desorption effect due to a flushing dry N$_2$ or helium gas stream. In Figure 2, the evolutions of the six individual water/uc populations versus the total water/uc loadings observed for different experimental conditions are compared at lower hydration states (0 < water/uc < 13). It is evident from this figure that the dehydration/ rehydration mechanism depends strongly on the experimental conditions.

3.3. Crystal Structure of the Cs$_{2.3}$H$_{1.1}$MFI·24H$_2$O Phase (RT 22 °C). As mentioned above, we are focusing our attention on the fully hydrated Cs$_{2.3}$H$_{1.1}$MFI·24H$_2$O phase, for which complementary calorimetric water adsorption energies are available. Thermal dehydration followed by isothermal rehydration at room temperature (22 °C, normal atmospheric pressure and ambient humidity) shows that this material sorbs 24 water molecules/uc. The XRPD refined value amounts to 24.1(7) water/uc, which is very close to the one observed by gravimetry.

The experimental conditions of the X-ray data collection as well as a few selected crystallographic parameters for this phase are reported in Table 3. The final atomic positions are given in Table 4, and the observed, calculated, and difference Rietveld plots are represented in Figure 3. Selected Cs−O(fr), Cs-water, and water−water distances are reported in Table 5. Once again we observe that in the hydrated phases most Cs−O(fr) distances are significantly longer than in the totally dehydrated parent phase. In Cs$_{2.3}$H$_{1.1}$MFI·24H$_2$O, the Cs3/uc population is very low, and this is why we omit this position from our schematic view of its crystal structure (Figure 4). In this case the complete hydration scheme consists of interconnected Cs$_2$(H$_2$O)$_5$ clusters (inner clusters) running through the straight channel ([010] axis direction) and Ow1-Cs1-(H$_2$O)$_4$ clustered water molecules (outer clusters) forming infinite chains trough the zigzag channels ([100] axis direction). In the case of Na(H$_2$O)$_n$ and Na$^+$(H$_2$O)$_n$ (1 < n < 6), a complete description of thermodynamically stable inner and outer cation/water molecular clusters is given in ref 16.
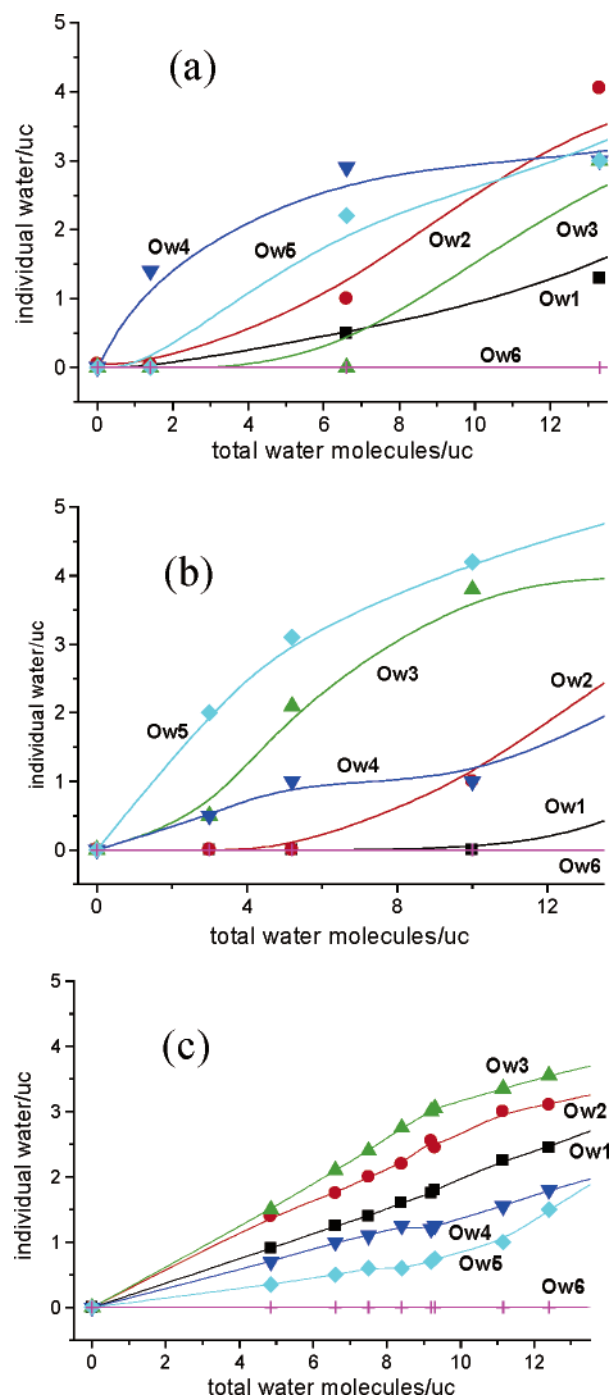

Figure 2. Populations of the individual water molecules/uc vs total water/uc (a) at increasing temperatures (see ref 9), (b) at room temperature (see ref 9), and (c) in dry N$_2$ flushed Cs$_x$H$_y$MFI·zH$_2$O phases at 26 °C during 6 h.

3824 *J. Phys. Chem. C, Vol. 111, No. 10, 2007*

Mentzen et al.

TABLE 3: Experimental and Selected Crystallographic Parameters for the $Cs_{2.3}H_{1.1}$MFI·24 H_2O Phase at Room Temperature (22 °C)

chemical formula	$Cs_{2.3}H_{1.1}Al_{3.4}Si_{92.6}O_{192}$·24 H_2O
space group	*Pnma*
powder diffractometer	IRCELYON, X'Pert Pro MPD
scan range (2θ, deg)	6.0083 − 80.0021
step size (2θ, deg)	0.0166765
wavelength (α_1/α_2) (Å)	1.540562/1.544330
profile function (U,V,W,As)	modified Lorentzian 2
counting time per step (s)	5
no. background points (linear interpolation)	48
no. of data points	4438
no. of contributing (reflections (*hkl*)	1695
no of refined structural parameters	144
a (Å)	20.0928(8)
b (Å)	19.9045(8)
c (Å)	13.3934(4)
$R_p/R_{wp}/R_{exp}/R(F^2)$ (%)	5.1/6.4/3.9/5.3
Si−O/O...O restraints (Å)	1.59/2.60 (∼ideal T_d)
refined Si − O range (Å)	1.567 − 1.625 (*mean* 1.596)
N − P + C	3032
sample temperature (°C)	22

4. Results from Adsorption Calorimetry

The evolution of the differential molar heats of sorption, corresponding to the $Cs_{2.3}H_{1.1}$ MFI/water system at 30 °C for increasing sorbate loadings, is represented in Figure 5. This sorption curve, obtained by high precision calorimetry, can be divided into five distinct water adsorption steps (I−V), the fifth one being further divided into two secondary steps (Va and Vb).

To interpret these calorimetric data, in particular their relationship with the crystal structure of $Cs_{2.3}H_{1.1}$MFI·24H_2O, and to establish the rehydration mechanism of the fully dehydrated sample step-by-step, several additional correlations need to be taken into account. Without those, a straightforward interpretation of the diffractometric plus calorimetric data is hardly feasible. Furthermore, when investigating structural features in microporous host/guest zeolitic complexes, preliminary computer simulations are usually invoked in order to get a guesstimated starting structural model for the zeolitic framework in the presence of extraframework species. We have already mentioned elsewhere[17−19] that the selection of a valid structural model (an actual refined zeolitic framemork) and of appropriate atom−atom potentials (Buckingham versus Lennard-Jones type models) are crucial for obtaining sensibly simulated sorbent/sorbate interaction energies. There are many examples of computer simulations which predicted a location of a sorbed molecule in total contradiction with experimentally observed results. These latter aspects are now illustrated and discussed in the following sections.

5. Discussion

5.1. Influence of the Si/Al Ratio on the Water Sorption Capacity in Cation Exchanged MFI Phases. In Figure 6, the water sorption capacities (water molecules/uc) versus Al/uc contents of some MFI-type phases (silicalite, cation-exchanged ZSM-5) are represented. The experimental values are obtained by dehydration/rehydration cycles using the thermogravimetric technique. Within experimental errors, the data points corresponding to all of the H−MFI zeolitic phases lie on a straight line, the average H_2O/uc versus Al/uc ratio being close to 8.5, which is far from a recently reported value (i.e., 4.0−4.4 H_2O/

TABLE 4: $Cs_{2.3}H_{1.1}$MFI·24H_2O at Room Temperature (22 °C)

atom	*x/a*	*y/b*	*z/c*	atom/uc[a]
T1	0.4234(4)	0.0605(5)	−0.3381(6)	
T2	0.3068(5)	0.0294(4)	−0.1855(6)	
T3	0.2798(4)	0.0604(5)	0.0346(6)	
T4	0.1199(4)	0.0615(5)	0.0273(7)	
T5	0.0717(4)	0.0291(4)	−0.1862(7)	
T6	0.1871(4)	0.0609(4)	−0.3256(6)	
T7	0.4236(4)	−0.1718(4)	−0.3264(7)	
T8	0.3074(4)	−0.1282(4)	−0.1819(6)	
T9	0.2743(4)	−0.1713(4)	0.0351(6)	
T10	0.1197(4)	−0.1725(4)	0.0301(6)	
T11	0.0716(4)	−0.1315(4)	−0.1859(7)	
T12	0.1875(4)	−0.1749(4)	−0.3217(6)	
O1	0.3724(6)	0.0546(8)	−0.2453(9)	
O2	0.3106(7)	0.0591(8)	−0.0760(6)	
O3	0.2000(3)	0.0581(8)	0.021(1)	
O4	0.0925(7)	0.0602(7)	−0.0829(6)	
O5	0.1152(5)	0.0581(8)	−0.2743(9)	
O6	0.2438(6)	0.0583(8)	−0.2437(9)	
O7	0.3752(6)	−0.1525(8)	−0.2342(9)	
O8	0.3057(7)	−0.1561(8)	−0.0712(6)	
O9	0.1966(3)	−0.1543(7)	0.033(1)	
O10	0.0935(8)	−0.1588(8)	−0.0795(7)	
O11	0.1169(5)	−0.1609(8)	−0.2725(9)	
O12	0.2451(6)	−0.1592(8)	−0.242(1)	
O13	0.3040(8)	−0.0495(3)	−0.182(1)	
O14	0.0780(8)	−0.0514(3)	−0.183(1)	
O15	0.4208(7)	0.1315(5)	−0.389(1)	
O16	0.4076(8)	0.0016(6)	−0.415(1)	
O17	0.4035(8)	−0.1294(6)	−0.4218(9)	
O18	0.1869(7)	0.1311(5)	−0.3817(9)	
O19	0.1946(8)	0.0003(5)	−0.401(1)	
O20	0.1975(8)	−0.1288(5)	−0.4165(8)	
O21	−0.0035(4)	0.0505(8)	−0.2076(1)	
O22	−0.0028(4)	−0.1534(8)	−0.208(1)	
O23	0.418(1)	−1/4	−0.350(1)	
O24	0.191(1)	−1/4	−0.361(1)	
O25	0.285(1)	−1/4	0.063(1)	
O26	0.108(1)	−1/4	0.057(1)	
Cs1	0.078(1)	1/4	0.877(1)	0.74(5)
Cs2	−0.020(1)	0.1492(7)	0.552(1)	1.43(2)
Cs3	0.22(1)1	1/4	0.99(2)	0.13(2)
Ow1	−0.0191(7)	1/4	0.715(1)	4 (f)[b]
Ow2	−0.167(1)	1/4	0.664(2)	4 (f)
Ow3	0.019(2)	1/4	0.419(2)	4 (f)
Ow4	0.131(1)	1/4	0.672(2)	3.4(2)
Ow5	0.033(2)	−0.004(1)	0.406(2)	6.5(3)
Ow6	0.206(1)	0.1792(7)	0.913(3)	2.2(2)

[a] T and O framework sites are fully occupied. U_{iso} (Å^2) of T/O/Cs/ water (Ow) = 0.0168(38)/0.024(9)/0.143(40)/0.13(1). [b] Fixed.

Al), where it is concluded on purely theoretical grounds that for each Al atom in the H−ZSM-5 framework, a charge compensating $H_9O_4^+$ (or H^+-$[H_2O]_4$) water cluster is formed[20] (H_2O/Al = 4). The data in Figure 6 show that for Al/uc < 4.5 the water sorption capacities of the Na and Tl-exchanged phases are close to those of the H−MFI phases. Cs-exchanged MFI materials have a lower water sorption capacity than the Li-exchanged samples. The H_2O/uc values corresponding to the Cs-exchanged phases investigated in this work and corresponding to Al/uc > 4.0 are not represented in Figure 6, since above this Al/uc limit the volume occupied by the Cs cations prevails over the increasing volume occupied by the sorbed water molecules. For Al/uc > 4, even the Na-exchanged materials sorb less than 8.5 H_2O/Al. This 4 Al/uc limit plays a crucial role in MFI-type zeolitic phases, and it is usually observed that, for higher aluminum/uc containing samples, increasing amounts of structure defects (essentially silanol groups and mesopores) are present in the samples investigated.
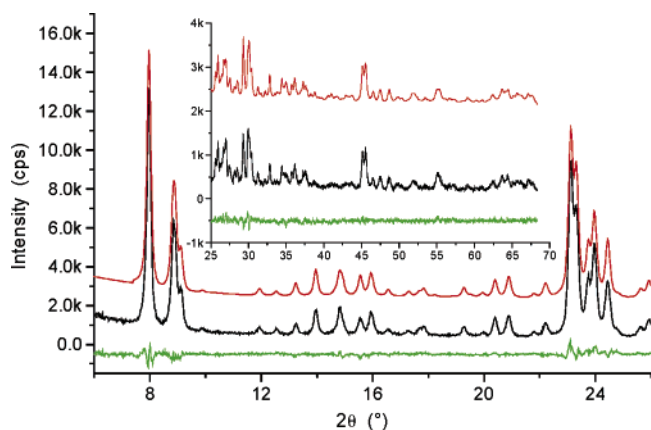
Hydrated Cs$^+$-Exchanged MFI Zeolites

J. Phys. Chem. C, Vol. 111, No. 10, 2007 **3825**

Figure 3. X-ray diffraction pattern of the fully hydrated $Cs_{2.3}H_{1.1}MFI \cdot 24H_2O$ phase at room temperature: calculated (upper trace), observed (middle trace), and difference (lower trace) patterns.

5.2. Influence of the Cation-Exchanged MFI Phase on the *p*-Xylene Sorption Capacity. The correlations existing between the chemical formula and the *p*-xylene sorption capacity of some cation-exchanged MFI-type phases are represented in Figure 7. For Al/uc < 4, the maximum sorbed *p*-xylene corresponds to 7.8−8.2 molecules/uc. This maximum sorption capacity is observed in most H−MFI-type zeolites.[21−23] The silicalite/*p*-xylene system has been extensively investigated, and the crystal structures of the silicalite/**2,4** and **8***p*-xylene/uc complexes are well established.[3,22−24]

For Al/uc < 4, all of the H−MFI phases investigated in the present work sorb eight *p*-xylene molecules/uc. For Na and Cs-exchanged MFI phases, the *p*-xylene sorption capacity is much lower than for the corresponding parent H−MFI samples. Since at saturation the *p*-xylene molecule fills almost completely the MFI channel system, there remains less and less space for the sorbing aromatic molecule when bulkier cations (Na, K, Rb, and Cs) are also present in the same accessible adsorption volume. For Cs-exchanged MFI-type phases, some *p*-xylene sorption capacities are reported in Figure 8. Point 1 corresponds to a highly siliceous silicalite (Si/Al ∼ 5000) and points 2 and 4 to literature data.[25] Point 3 has been deduced from differential calorimetric adsorption measurements corresponding to the $Cs_{2.3}H_{1.1}ZSM-5$/*p*-xylene system. The estimated *p*-xylene/uc loadings in Cs-exchanged MFI materials can be calculated by the $8.02 - 0.862 \times Cs/uc - 0.162 \times (Cs/uc)^2$ second-order regression curve ($R = 0.98$). All of the experimental points lie close to this regression curve, which might be used as a benchmark for testing well-crystallized Cs-exchanged MFI-type zeolites.

In the case of a Li-exchanged phase, the calorimetric curve shows that the apparent sorption capacity exceeds 8 *p*-xylene molecules/uc. Chemical analysis and N_2 adsorption isotherms (BJH pore-distribution method) reveal the existence of meso-porous domains in $Li_{1.4}H_{2.0}ZSM-5$, and that its microporous volume decreases to 0.143 mL/g, instead of the usual 0.19 mL/g value for a so-called defect free MFI material.[26] As a result, more than 8 *p*-xylene/uc are adsorbed: eight molecules in the strictly microporous crystalline part and the excess in the noncrystalline mesoporous part. It must be emphasized that crystal structure determinations permit us to locate only sorbate molecules in the micropores; the additional sorbed molecules, which reside in the mesopores, being characterized by complementary experimental techniques only (isotherms, calorimetry, and infrared among others).

In Figure 7, two data points corresponding to *p*-xylene sorbed H−MFI phases are marked by an asterisk. These two points correspond to samples presenting substantial framework structure defects. In the case of defect free H−MFI samples (0 < H/uc < 4.0 ± 0.1), and only in this case, *p*-xylene sorption measurements are a very convenient and simple way to test the crystallinity of the zeolitic H−MFI phases: the sorption isotherms *must* correspond to 8.0 ± 0.2 *p*-xylene molecules/uc. During our *p*-xylene adsorption measurements an uncommon observation happened: it was possible to force *p*-xylene sorption into already water saturated H−MFI samples. Such a result is illustrated in Figure 9. First, water is isothermally adsorbed in a dehydrated $H_{3.3}MFI$ sample (heating up to 450 °C followed by cooling down at room (22 °C) temperature); the water sorption capacity amounts to 28.4 H_2O/uc, in good agreement with the straight correlation line in Figure 6 (8.6 H_2O/Al). Second, after water sorption equilibrium is attained (125 min), a small crucible containing liquid *p*-xylene is placed close to the $H_{3.3}MFI \cdot 28.4H_2O$ sample and the mass take-up monitored for a while. After 4 h, a new equilibrium corresponding to 7.8-(1) *p*-xylene molecules/uc is attained. In order to check this experiment, a second *p*-xylene desorption/resorption (heating/cooling/sorption) run is performed: the final weight corresponds to exactly the same 7.8(1) *p*-xylene molecules/uc sorption capacity. Everything happens as if the nonpolar aromatic hydrocarbon expels the polar water molecule. This phenomenon is also easily observed by routine X-ray powder diffractometry. In fact, the diffraction patterns corresponding to *p*-xylene saturated H−MFI phases are very characteristic and strikingly different from those observed in the case of the parent water saturated phases. Accordingly, the crystallinity of a ZSM-5 zeolite might be conveniently estimated by simply inspecting the XRPD profile corresponding to the *p*-xylene saturated parent H−MFI phase.

5.3. Influence of the Proton in H−MFI Phases on Benzene Sorption Calorimetry. The differential molar adsorption calorimetric curves represented in Figure 10 correspond to silicalite·**1**benzene and four H−MFI·*n*benzene (0.6 < *n* < 4.2) systems.[27,28] The data points corresponding to the H−MFI phases are obtained by digitizing the experimental curves reported in ref 27 and those corresponding to silicalite from ref 28.
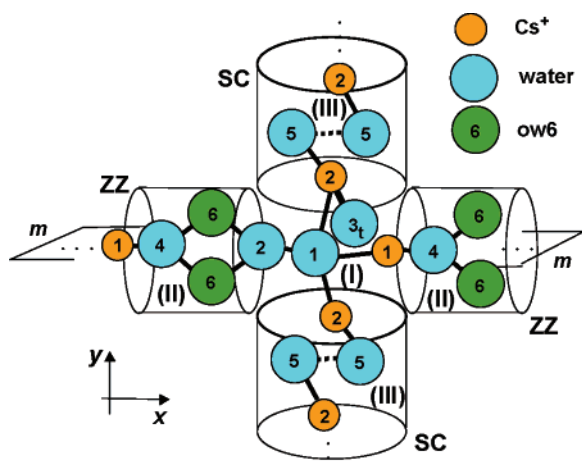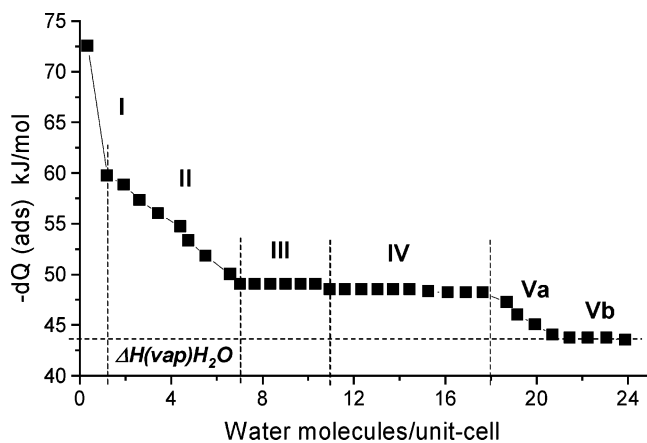
Thamm's silicalite sample (cyan colored diamonds in Figure 10) contains 0.96 silanol/uc.[28] At lower benzene loadings (0 < benzene/uc < 3.5), the two curves corresponding to silicalite and $H_{0.6}$-ZSM-5 are almost superposed and a first adsorption heat plateau at −57.5 kJ/mol is attained for 0.9−1.0 benzene/uc. Accordingly, the steep energy decrease (∼ −83 to 57.5 kJ/mol) observed in the 0−1.0 benzene/uc range is attributed to the very energetic silanol (−OH) or proton (H)/sobate interactions. For the calorimetric curves corresponding to the $H_{1.1}$-ZSM-5, $H_{2.1}$-ZSM-5, and $H_{4.2}$-ZSM-5/benzene systems, the horizontal plateaus are approximatively reached for 1.1, 2.1, and 4.2 benzene/uc, respectively. As a consequence, the observed higher adsorption energy drops are directly correlated with the silanol/uc and/or the proton/uc concentrations in the investigated phases. Interpretation of the calorimetric curve corresponding to the 4 < benzene/uc < 8 loaded samples is discussed in the next section (5.4).

5.4. Influence of the Presence of Silanol Defects in Sorption Calorimetry. In Figure 11, the differential molar sorption heats corresponding to two different silicalite/benzene systems are represented. In this figure, the squares and circles correspond to Thamm's (Sil**1**) silicalite (see refs 27 and 28) and to a nearly defect free (silanol < 0.1/uc) sample (Sil**2**) prepared in fluoride medium, respectively. Zeolitic MFI-type
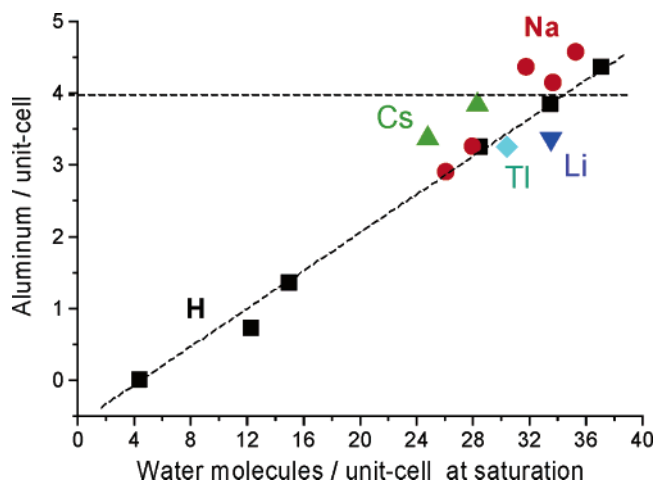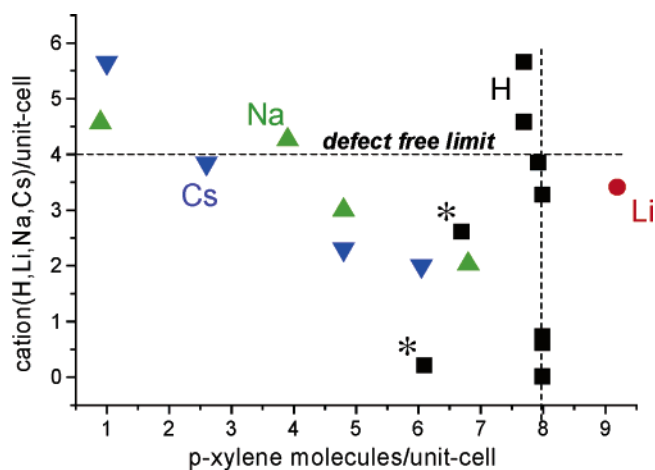
TABLE 5: Selected Cation to Framework−Anion Bonds and Cation to Water, Water−Water, and Water−Framework Distances (Å) in the $Cs_{2.3}H_{1.1}MFI\cdot24H_2O$ Phase at 22 °C[a]

atom pair	distance	atom pair	distance	atom pair	distance
Cs1−O17	**3.62**(2)	Cs2−O21	3.78(2)	Cs3−O3	3.86(2) × 2
Cs1−O26	3.84(2)	Cs2−O2	3.86(2)		
Cs1−O4	3.82(2)	Cs2−O1	3.86(2)		
Cs1−O15	3.95(3)				
Cs1−Ow6	2.96(2) × 2	Cs2−Ow5	2.95(3)	Cs3−Ow2	3.06(3)
Cs1−Ow1	2.92(2)	Cs2−Ow3	**2.80**(2)		
Cs1−Ow4	2.95(2)	Cs2−Ow1	2.96(2)		
Ow1−Ow2	3.06(3)	Ow2−Ow6	3.09(3) × 2	Ow6−Ow6	*2.82*(3)
Ow1−Ow4	3.08(3)	Ow5−Ow5′	2.85(2)[b]	Ow6−Ow2	3.09(3)
Ow3−O22	3.43(3) × 2	Ow6−O17	3.09(3)	Ow6−O20	3.16(3)
Ow5−O2	3.33(3)	Ow6−O4	3.28(3)	Ow6−O2	3.19(3)
Ow5−O21	*2.88*(3)	Ow6−O3	*2.81*(2)		

[a] The shortest cation-framework or cation-water distances are in bold characters, and the most probable hydrogen bonds are in italics. Only distances less than 3.9 Å are given. [b] Ow5′ is the symmetry-related Ow5 site (through the inversion center).

Figure 4. Simplified view of the $Cs_{2.3}H_{1.1}MFI\cdot24H_2O$ crystal structure. In this figure the Cs3 site is omitted for clarity's sake (see text).

Figure 6. Correlation between the water sorption capacities and the Al/uc content in cation-exchanged MFI-type phases.

Figure 5. Differential molar adsorption calorimetry curve observed for the $Cs_{2.3}H_{1.1}MFI$/water system.

Figure 7. *p*-Xylene sorption capacities of cation-exchanged MFI-type zeolitic materials.

materials synthesized in fluoride medium (using TPAF as structure directing organic template) are known to contain a much lower structural defect concentration than those synthesized by the usual alkaline way (using TPABr as structure directing organic template in the presence of NaOH). Furthermore, calcination of as-synthesized MFI-TPAF zeolites yields directly the H−MFI form, whereas calcination of MFI-TPABr zeolites yields the Na−MFI form, which has first to be ammonium-exchanged, in order to get (after calcination) the H−MFI form, before any other cation-exchange is performed. The calorimetric curves drawn in Figure 11 clearly show the undesired side-effects caused by the presence of silanol groups

in the case of Sil**1**/benzene interactions. These effects are particularly evident in the 0−1, 3.5−5, and 6−8 benzene/uc sorbate loading ranges. As already noticed (section 5.3), the high-energy 0 < benzene/uc < 1 domain corresponds to the specific interactions between the silanol groups and benzene. The strong sorbate/silanol interactions observed at lower fillings are explained in section 5.5.2. For Sil**1**, the 3.5−5 benzene/uc domain corresponds to the monoclinic/orthorhombic $P2_1/n11$ → *Pnma* solid-state phase transition, which should normally take place at 4 benzene/uc, as it is observed for the Sil**2** silicalite (the first energy minimum is observed at exactly 4 benzene/
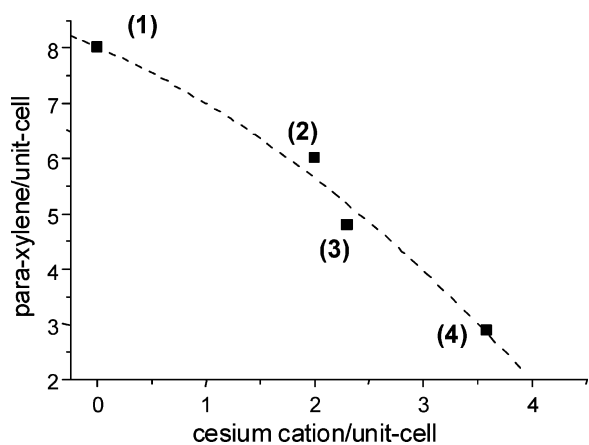
Hydrated Cs⁺-Exchanged MFI Zeolites

J. Phys. Chem. C, Vol. 111, No. 10, 2007 **3827**

Figure 8. Correlation between the *p*-xylene sorption capacities and the Cs/uc content in MFI-type phases.
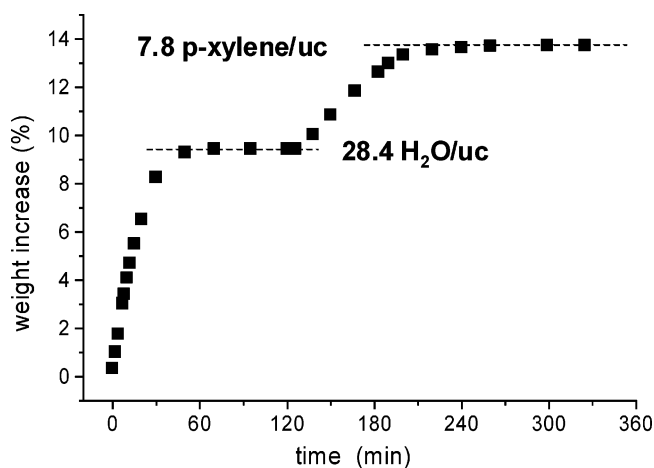

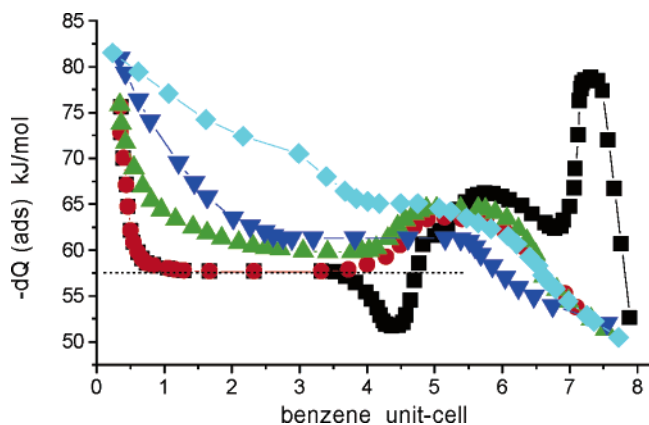**Figure 9.** Water/*p*-xylene co-adsorption in a H$_{3.3}$MFI phase.

Figure 10. Differential molar heats of sorption of benzene in H$_x$-ZSM-5 phases and silicalite at 28 °C. For $H = 4.2$ (diamonds), 2.1 (triangles down), 1.1 (triangles up), and 0.6 (circles). Silicalite: squares.

uc). In the 6−8 benzene/uc domain, the silicalite/benzene interactions are extremely complex. The complexity of the silicalite/benzene system for these higher sorbate concentrations has been investigated by solid-state ²⁹Si *mas*NMR[30] and X-ray diffractometry,[31] but as of yet, no definitive interpretation describing the intimate sorbent/sorbate interactions is available. Nevertheless, all of the published results consider that, for the 6−8 benzene/uc concentration range, the silicalite/benzene system presents several multiphased domains, involving several framework symmetries ($P2_1/n11$, *Pnma*, $P2_12_12_1$, and probably $Pn2_1a$). This silicalite/benzene system is currently under investigation, using the combined X-ray and neutron diffraction
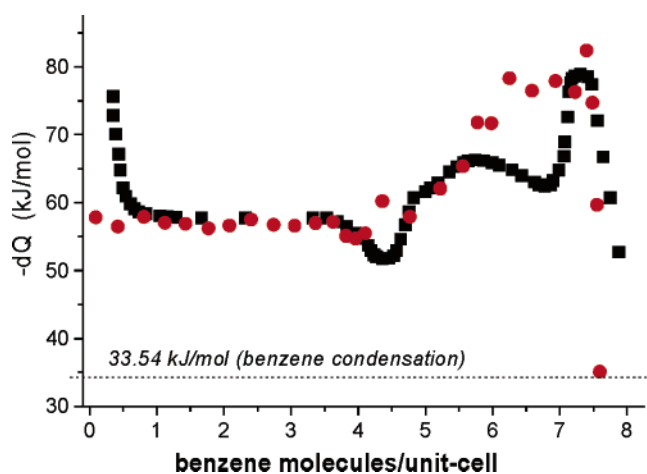

Figure 11. Differential molar heats of sorption of benzene in two silicalite samples. Squares: silicalite containing 0.96 silanol/uc − circles: defect free silicalite.
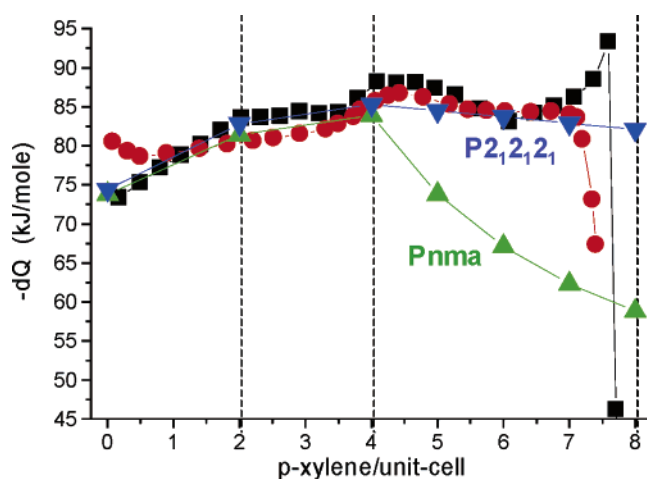

Figure 12. Silicalite/*p*-xylene system. Circles: calorimetric curve from ref 28 (0.96 silanol/uc). Squares: defect free silcalite. Triangles down: simulated for the $P2_12_12_1$ space group (*p*-xylene/uc > 4). Triangles up: simulated for the *Pnma* space group (*p*-xylene/uc > 4).

techniques, high precision molar adsorption calorimetry, solid-state ²⁹Si *mas*NMR spectroscopy and computer simulations (MM).[32]

5.5. Influence of the Structural Model in Computer Simulations. The importance of using actual framework structures in computer simulations concerning MFI/sorbate systems has already been emphasized.[8,9] This will now be further illustrated by two examples corresponding to a silicalite/*p*-xylene system and the H$_{3.3}$-MFI·2.5C$_6$D$_6$ benzenate.

5.5.1. Simulation of a Phase Transition. In Figure 12, four calorimetric curves are represented. The circles (red) and squares (black) correspond to the already reported curve in ref 28 (digitized data) and the Sil**2**/*p*-xylene system, respectively. The up (green) and down (blue) triangles in the 4−8 *p*-xylene/uc range correspond to the computer simulated curves using the *Pnma* (**O1**) and $P2_12_12_1$ (**O2**) framework symmetries, respectively. The simulated curves clearly show that the best fit is obtained when the *actual* $P2_12_12_1$ framework symmetry is used.[3]

5.5.2. Simulation of Specific Proton Interactions. Computer simulations of proton (acidic sites) locations in H−MFI materials are reported in refs 33 and 34. They show that the protons are not distributed randomly over the 26 possible sites in the H−MFI materials (26 O(fr) atoms, orthorhombic *Pnma* space group framework symmetry). However, no definitive H locations
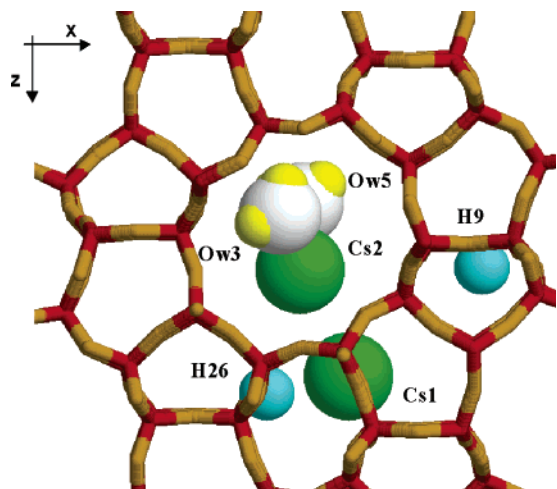
3828 *J. Phys. Chem. C, Vol. 111, No. 10, 2007*

Mentzen et al.

Figure 13. Extraframework species present at very low water loadings (0–1.1 water/uc).

TABLE 6: Estimated Adsorption Energies for the Cs$_{2.3}$H$_{1.1}$MFI/Water System at Very Low Sorbate Loadings (0 < Water/uc < 1.1)

sites concerned	energy (-kJ/mol)	Cs–water distance (Å)
Cs2 + Ow5	63.2	2.98
Cs2 + Ow3	61.8	3.00
Cs2 + Ow5 + H9	65.1	2.99
Cs2 + Ow5 + H26	67.1	3.02
Cs2 + Ow5 + H9 + H26	68.5	2.98
Cs2 + Ow3 + H9	64.1	3.00
Cs2 + Ow3 + H26	65.1	3.01
Cs2 + Ow3 + H9 + H26	67.8	3.01

could be unambiguously confirmed.[33] In this static energy minimization study (rigid framework, proton, and benzene species), out of the 26 theoretically possible proton locations (O(fr)-H = 1.0 Å), those corresponding to an enhancement of the H−MHI/benzene potential interactions are bonded to the O1, O8, O11, and O18 framework O(fr) atoms. Most of these O(fr) atoms are bonded to the T2 or T12 sites (T corresponding to possible Si,Al tetrahedral substitution site in the MFI framework). In other words, in ref 33, the proton locations have not been optimized. If the framework and the protons are refined from diffraction data (with geometrical restraints on the framework Si−O(fr)/O(fr)···O(fr) and O(fr)−H distances, the benzene molecules being considered as rigid bodies), among the 26 possible protons in the H$_{3.3}$−MFI·2.5C$_6$D$_6$ complex, only two protons (H atoms) corresponding to H9 (bonded to O9, close to T9 and T10) and H26 (bonded to O26, twice close to T10) yield sensible refined populations. The T9 and T10 metallic framework sites correspond to small 4-membered rings in the MFI crystal structure, and it is commonly accepted that in MFI materials acid sites are close to these T sites (see Table 10 in ref 8 and references therein). The refined populations of the three independent deuterobenzene molecules which are disordered in the channel intersection[35] are 0.71(3)/1.04(3)/0.75(2) for the benzene species in three different orientations, respectively. The refined populations of the two characterized protons are 1.8(2) and 1.5(2) for H9 and H26, and their positional parameters are x,y,z = 0.315, 0.124, and 0.589 and −0.072, 1/4, and 0.908, respectively. These latter results and those reported in the preceding sections will now be used in the interpretation of the hydration mechanism of Cs$_{2.3}$H$_{1.1}$MFI.

5.6. Hydration Mechanism of Cs$_{2.3}$H$_{1.1}$MFI. It will now be shown how the discussions reported in the preceding sections contribute to a better understanding of the hydration mechanism of the Cs$_{2.3}$H$_{1.1}$MFI phase, by interpreting the complementary X-ray diffraction and adsorption calorimetry data. The first 0 < water/uc < 1.1 adsorption domain (Figure 5, step I), corresponding to a steep energy decrease (−72.5 to −60 kJ/mol) is attributed to specific interactions between the first adsorbed water molecules and the 1.1/uc protons of the chemical formula in the investigated Cs$_{2.3}$H$_{1.1}$MFI phase (possible Al−O(fr)-H-OH$_2$ interactions). Such dramatic energy drops at lower sorbate fillings are frequently observed when polar or aromatic molecules are adsorbed in zeolitic MFI phases presenting protons and/or silanol groups.[27,28,36−38] Figure 13 represents the Cs$_{2.3}$H$_{1.1}$MFI/water system at very low sorbate loadings: the

Cs2,Cs1 cations and the H9,H26 protons are in place, and the first water Ow5 and Ow3 molecules start to be adsorbed. In the case of the Cs$_{6.6}$H$_{0.3}$MFI/water system,[9] the best model for the progressive loadings of the six independent water molecules at room temperature are represented in Figure 2b, and we assume that this model is also valid for the Cs$_{2.3}$H$_{1.1}$-MFI/water system. According to this Figure, the very first water species adsorbed at lower loadings are Ow5, Ow3, and Ow4. The estimated adsorption energies for several cation/proton/water configurations (in this simulation only the Ow3 and Ow5 water species are considered at zero-filling) are calculated by using the molecular mechanics model (MM) detailed in refs 8 and 9. In these calculations, the MFI framework, the Cs cations, and the H protons are fixed (actual refined atomic positions given in sections 3.3 and 5.5.2), and the water molecules are free to move toward their energy minimized locations. The calculated interaction energies are reported in Table 6. If the proton/water interactions are neglected, the estimated adsorption energy is −62.5 kJ/mol (mean of the Cs2+Ow5 and Cs2+Ow3 interactions). This energy is very close to the value extrapolated at zero-filling (−61.5 kJ/mol, if we discard the energy drop observed for step I). If the effects of the protons on the adsorption mechanism are now taken into account, the calculated adsorption energies are significantly higher than the zero-filling extrapolated value. Even if the highest estimated energies (−67.8 and −68.5 kJ/mol) are somewhat lower than the highest observed value (−72.5 kJ/mol), the specific action of the protons is correctly simulated.

The second energy drop (−60 to −49.5 kJ/mol) corresponds to the 1.1 < water/uc < 7.1 hydration range (Figure 5, step II). At 7.1 water/uc, the Cs2 cation and the Ow5 + Ow3 water species, which are directly bonded to this cation, initiates the overall CsH(H$_2$O)$_2$ hydration scheme, corresponding to the formation of a first Cs/water cluster, where the water molecules are in the first coordination sphere of the cation. The linear energy drop observed in step II corresponds to the simultaneous effects of decreasing proton/water interactions and of increasing unfavorable water/water interactions, which are due to the progressive crowding of the incoming sorbate molecules. These unfavorable water/water interactions in growing cation/(H$_2$O)$_n$ clusters (cation = Na, Mg, Ca, and Sr and 1 < n < 6) is a known effect.[16,39−41]

The third hydration step III corresponds to a first plateau (−49.5 to −48.5 kJ/mol) observed for the 7.1 < water/uc < 10.5 loadings. As for the preceding steps, at step III the 10.5−7.1 = 3.4 H$_2$O/uc water content correlates with the Al/uc value, as it is the Al content of this phase. At 10.5 water/uc, the Cs1 cation is hydrated by Ow4, and the overall hydration scheme corresponds to Cs,H(H$_2$O)$_3$. Step IV (−48.5 to −47.5 kJ/mol) corresponds to a second plateau observed for 10.5 < water/uc < 18 loadings. At 18 water/uc, the second coordination spheres of Cs2 and Cs1 are also hydrated, and the overall hydration

TABLE 7: Hydration Mechanism of the Cs$_{2.3}$H$_{1.1}$MFI Phase

hydration step[a]	water/uc range	overall scheme	involved species
I	0−1.1	(O)-H/water	mainly Ow5, Ow3, H9, H26
II	1.1−7.1	Cs,H(H$_2$O)$_2$	+ Cs2, Ow5 and Ow3
III	7.1−10.5	Cs,H(H$_2$O)$_3$	+ Cs1 and Ow4
IV	10.5−18	Cs,H(H$_2$O)$_5$	+ Cs2, Ow1 and Cs1, Ow1
V (**a** and **b**)	18−23.9	Cs,H(H$_2$O)$_7$	+ Cs3, Ow2, Ow4, Ow6 + long range interactions

[a] See Figure 5.

scheme is now Cs,H(H$_2$O)$_5$. The last hydration domain (steps Va and Vb) corresponds to the 18 < water/uc < 23.9 domain. In this step, the very low populated Cs3 cation starts to be hydrated by Ow2, Ow4, and Ow6. The two Va (−47.5 to −43.5 kJ/mol, 18 < water/uc < 21.5) and Vb (−43.5 kJ/mol, 21.5 < water/uc < 23.9) steps observed in this final hydration range, might be due to the combined or successive effects of the energetically low Cs3/water interactions and the formation of the (H$_2$O)$_4$ cluster in the zigzag channel sections. Finally, the overall hydration scheme is CsH(H$_2$O)$_7$, and the adsorption energy reaches the vaporization enthalpy of water (−43.5 kJ/mol at 30 °C). According to our interpretations, the water saturation capacity of the Cs$_{2.3}$H$_{1.1}$MFI phase is 3.4 × 7 = 23.8 water/uc, which is very close to the observed value (23.9). The complete water hydration mechanism is summarized in Table 7.

6. Conclusions

In the present work, it is shown that the correlations existing between the individual Cs/uc species versus total Cs/uc content in the totally dehydrated parent Cs$_x$H$_y$MFI phases (five distinct Cs cationic species), can be extended to their corresponding hydrated Cs$_x$H$_y$MFI·zH$_2$O phases (three distinct Cs species) for 0.7 < Cs/uc < 7.7. This proves the unique Cs cation incorporation mechanism for both the investigated Cs-exchanged series, i.e., the dehydrated[8] and their fully hydrated samples.[9] The dehydration mechanism of one of them, i.e., Cs$_{6.6}$H$_{0.3}$MFI· 28H$_2$O, has been investigated by in situ and ex situ X-ray powder diffraction, and its progressive hydration mechanism elucidated by solely interpreting the diffraction patterns corresponding to progressively dehydrated phases by the Rietveld structure refinement method.[9] Even if this structure refinement methodology yields a complete step-by-step description of the dehydration process (locations of cations and water species) at increasing (in situ runs, Figure 2a) and at room temperatures (ex situ runs, Figure 2b), the role played by the 0.3 protons of the formula cannot precisely be interpreted. The only sample of our Cs$_x$H$_y$MFI·zH$_2$O series (0.7 < x < 7.7−0.3 < y < 5.3−4 < z < 32), for which additional high precision molar water adsorption calorimetry data are available, corresponds to the Cs$_{2.3}$H$_{1.1}$MFI·24H$_2$O phase. This prompted us to solve its crystal structure (see section 3.3) and try to interpret the evolution of the experimental adsorption energies versus water loadings, by using the results of the crystal structure determination. It appears that this cannot be done on the sole basis of the structural information, since the adsorption calorimetry is prone to detect very subtle and unsuspected sorbent/sorbate interactions (see section 5.4), which remain undetected when only the powder diffraction technique is used. It also appears that for a straightforward interpretation of the calorimetric curve, the knowledge of additional physicochemical and structural correlations are needed. These correlations are discussed in sections 5.1 to 5.5. On the basis of these correlations and of the crystal structure data, the complete hydration mechanism of the Cs$_{2.3}$H$_{1.1}$MFI phase is now completely established. This work

illustrates all the benefit one may get from additional adsorption calorimetry data, the ideal case being a combined investigation using both the diffraction and the calorimetric techniques performed on the very same sample.

As mentioned in section 5.4, besides experimental adsorption calorimetry, another very valuable investigation technique in zeolitic host/guest complexes, is the solid-state ^{29}Si *mas*NMR spectroscopy. This technique, which is extensively used in the case where the host structure is silicalite[42,43] (<~0.1 Al/uc, ^{29}-Si *mas*NMR peaks), yields practically no details in the case of ZSM-5 materials. In defect free silicalite no charge compensating protons are present (no Al framework sites), but as shown in section 5.5 and refs 44 and 48, in some commercial zeolitic samples, undesired silanol defects are heavily perturbating the investigated structural properties of the material.

As a general conclusion from the present work and two previous articles[8,9] concerning a research on Cs-exchanged zeolitic MFI-type host−guest complexes, we would like to emphasize the following points:

(1) In MFI-type materials the charge compensating Cs cations are located on a restricted number of sites (five in the dehydrated samples and three in the hydrated phases), and in the presence of sorbed polar or nonpolar molecules these cations do not cooperatively migrate or assemble and agglomerate themselves in order to only yield a single coordination center.[44−48]

(2) Cs-cation exchange in MFI-type materials leads to an unexpected flexibility of the zeolitic framework. This flexibility is quantified by the variation of the ellipticity (ϵ, present work and refs 8 and 9) of the straight and/or zigzag channel 10-R pore-openings[49,50] (the $1/s$ ratio in refs 49 and 50). Even if the MFI-type framework (the 10-ring openings) is less flexible than in RHO-type materials (the 8-ring openings),[51] the absolute framework oxygen displacements are comparable. During the silicalite·4p-xylene (*Pnma*) silicalite·8p-xylene[3] ($P2_12_12_1$) solid-state phase transition, the orientation of the major-axis of the elliptical straight-channel 10-ring section is rotated by ~69° and the O1⋯O7/O5⋯O11 displacements correspond to 1.3/1.0 Å, respectively.[3,22] These displacements are even greater if we compare the silicalite·8p-xylene[3] and the silicalite·4naphthalene (*Pnma*)[52,53] structures (O1⋯O7/O5⋯O11 displacements = 1.64/ 1.63 Å, respectively). In RHO-type materials, the maximum framework O⋯O displacements in the 8-ring channel sections are close to 1.2 × 2.0 Å, and the mean displacement value (1.6 Å) is comparable to that observed in silicalite/sorbate complexes.

(3) Whenever possible, and particularly if unambiguous results are aspired to, crystal structure investigations concerning zeolitic host−guest complexes should always combine several experimental techniques, at least diffraction (by using X-ray and/or neutron beam-lines on powdered samples or single crystals) yielding actual framework structures, differential molar adsorption calorimetry (for detecting subtle sorbent/sorbate interactions) and solid-state NMR spectroscopy (in the case of silicon rich MFI materials).

Mentzen et al.

and A. Tissler, Mainz (Germany) for the MFI samples prepared in fluoride, in classical (with template) alkaline and in templateless alkaline media, respectively.

Supporting Information Available: Refined atomic positional parameters for some fully hydrated $Cs_{0.7}H_{0.7}MFI \cdot 16H_2O$, $Cs_{2.0}H_{1.6}MFI \cdot 19H_2O$, $Cs_{3.2}H_{5.0}MFI \cdot 20H_2O$, and $Cs_{7.7}H_{1.1}MFI \cdot 31H_2O$ phases (Tables 1S−4S), and some selected dry N_2 flushed and partially hydrated $Cs_{1.6}H_{2.2}MFI \cdot 4.5H_2O$, $Cs_{2.3}H_{1.1}$-$MFI8.4H_2O$, $Cs_{2.9}H_{5.3}MFI \cdot 6.5H_2O$, and $Cs_{5.4}H_{3.4}MFI \cdot 9H_2O$ phases (Tables 5S−8S) are given. This material is available free of charge via the Internet at http://pubs.acs.org.

References and Notes

(1) Baerlocher, Ch.; Meier, W. M.; Olson, D. H. *Atlas of Zeolite Framework Types*, 5th ed.; Elsevier: Amsterdam, 2001.

(2) van Koningsveld, H.; van Bekkum, H.; Jansen, J. C. *Acta Cryst.* **1987**, *B43*, 127−132.

(3) van Koningsveld, H.; Tuinstra, F.; van Bekkum, H.; Jansen, J. C. *Acta Cryst.* **1989**, *B45*, 423−431.

(4) Mentzen, B. F. *C. R. Acad. Sci. Ser. II* **1988**, *307*, 559−564.

(5) Mentzen, B. F.; Lefèbvre, F. *Mater. Res. Bull.* **1997**, *32*, 813−821.

(6) Mentzen, B. F.; Lefèbvre, F. *J. Chim. Phys.* **1998**, *95*, 1052−1067.

(7) Mentzen, B. F.; Tuel, A.; Bayard, F. *Microporous Mesoporous Mater.* **2006**, *93*, 171−179.

(8) Mentzen, B. F.; Bergeret, G.; Emerich, H.; Weber, H. P. *J. Phys. Chem. B* **2006**, *110*, 97−106.

(9) Mentzen, B. F.; Bergeret, G.; Emerich, H.; Weber, H. P. *J. Phys. Chem. B* **2006**, *110*, 13741−13752.

(10) Wiles, D. B.; Young, R. A. *J. Appl. Crystallogr.* **1981**, *14*, 149−151.

(11) Toby, B. H. EXPGUI, a graphical user interface for GSAS, *J. Appl. Crystallogr.* **2001**, *34*, 210−213.

(12) Rakhmatkariev, G. U. *Clays Clay Miner.* **2006**, *54*, 405−410.

(13) Hunger, J.; Beta, I. A.; Böhlig, H.; Ling, Chapter; Jobic, H.; Hunger, B. *J. Phys. Chem. B* **2006**, *110*, 342−353.

(14) Hunger, B.; Heuchel, M.; Matysik, S.; Beck, K.; Einicke, W. D. *Thermochim. Acta* **1995**, *269/270*, 599−611.

(15) Hunger, B.; Matysik, S.; Heuchel, M.; Geidel, E.; Toufar, H. J. *Therm. Anal.* **1997**, *49*, 553−565.

(16) Hashimoto, K.; Morokuma, K. *J. Am. Chem. Soc.* **1994**, *116*, 11436−11443.

(17) Mentzen, B. F.; Bosselet, F. C. *R. Acad. Sci. Ser. II* **1989**, *309*, 539−545.

(18) Mentzen, B. F.; Lefèbvre, F. *Mater. Res. Bull.* **1995**, *30*, 613−620.

(19) Cundari, T. R. *Computational Organometallic Chemistry*; Marcel Dekker Inc: New York, 2001; p 264.

(20) Olson, D. H.; Haag, W. O.; Borghard, W. S. *Microporous Mesoporous Mater.* **2000**, *35−36*, 435−446.

(21) Olson, D. H.; Kokotailo, G. T.; Lawton, S. L.; Meier, W. M. *J. Phys. Chem.* **1981**, *85*, 2238.

(22) Mentzen, B. F.; Gélin, P. *Mater. Res. Bull.* **1995**, *30*, 373−380.

(23) Gélin, P.; Dutel, J. F.; Mentzen, B. F. *Microporous Mater.* **1995**, *4*, 283−290.

(24) Mentzen, B. F.; Bosselet, F. *Mater. Res. Bull.* **1988**, *23*, 227−235.

(25) Mentzen, B. F.; Gélin, P. *Mater. Res. Bull.* **1998**, *33*, 109−116.

(26) Flanigen, E. M.; Bennett, J. M.; Grose, R. W.; Cohen, J. P.; Patton, R. L.; Kirchner, R. M.; Smith, J. V. *Nature* **1978**, *271*, 512−516.

(27) Thamm, H.; Jerschkewitz, H.-G.; Stach, H. *Zeolites* **1988**, *8*, 151−153.

(28) Thamm, H. *J. Phys. Chem.* **1987**, *91*, 8−11.

(29) Guth, J. L.; Kessler, H.; Wey, R. *Proceedings of the 7th International Zeolite Conference*; Elsevier: Amsterdam, 1986; p 121.

(30) Fyfe, C. A.; Strobl, H.; Kokotailo, G. T.; Kennedy, G. J.; Barlow, G. E. *J. Am. Chm. Soc.* **1988**, *110*, 3373−3380.

(31) Sacerdote-Perronet, M.; Bosselet, F.; Bouix, J.; Mentzen, B. F. *C. R. Acad. Sci. Ser. II* **1991**, *312*, 1513−1520.

(32) Mentzen, B. F.; Rakhmatkariev, G. U.; Lefèbvre, F. in preparation.

(33) Mentzen, B. F.; Sacerdote-Peronnet, M. *Mater. Res. Bull.* **1994**, *29*, 1341−1348.

(34) Toby, B.; Purnall, S.; Hu, R.; Peters, A.; Olson, D. H. *Proceedings of the 12th International Zeolite Conference, July 5−10, 1998, Baltimore, Maryland, U.S.A.* 1999; Vol. IV, pp 2413−2418.

(35) Sacerdote-Peronnet, M.; Mentzen, B. F. *Mater. Res. Bull.* **1993**, *28*, 767−774.

(36) Akhmedov, K. S.; Rakhmatkariev, G. U.; Dubinin, M. M.; Isirikyan, A. A. *Izvest. Akad. Nauk SSSR* **1987**, *8*, 1717−1721.

(37) Dubinin, M. M.; Rakhmatkariev; G. U.; Isirikyan, A. A. *Izvest. Akad. Nauk SSSR* **1989**, *9*, 2117−2120.

(38) Boddenberg, B.; Rakhmatkariev, G. U.; Greth, R. *J. Phys. Chem. B* **1997**, *101*, 1634−1640.

(39) Bauschlicher, C. W.; Langhoff, S. R. Jr.; Partridge, H. *J. Chem. Phys.* **1991**, *95*, 5142−5148.

(40) Bauschlicher, C. W.; Sodupe, M., Jr.; Partridge, H. *J. Chem. Phys.* **1992**, *96*, 4453−4463.

(41) Kochanski, E.; Constantin, E. *J. Chem. Phys.* **1987**, *87*, 1661−1665.

(42) van Koningsveld, H.; Jansen, H.; van Bekkum, H. *Zeolites* **1990**, *10*, 235−241.

(43) Mentzen, B. F. *Mater. Res. Bull.* **1995**, *30*, 1333−1340.

(44) Moissette, A.; Marquis, S.; Gener, I.; Brémard, C. *Phys. Chem. Chem. Phys.* **2002**, *4*, 5690−5696.

(45) Moissette, A.; Brémard, C. *Microporous Mesoporous Mater.* **2001**, *47*, 345−357.

(46) Nachtigallova, D.; Nachtigall, P.; Sierka, M.; Sauer, J. *Phys. Chem. Chem. Phys.* **1999**, *1*, 2019−2026.

(47) Nachtigallova, D.; Nachtigall, P.; Sauer, J. *Phys. Chem. Chem. Phys.* **2001**, *3*, 1552- 1559.

(48) Mentzen, B. F. *C. R. Chimie* **2005**, *8*, 353−368.

(49) van Koningsveld, H.; Jansen, J. C.; de Man, A. *J. M. Acta Cryst.* **1996**, *B52*, 131−139.

(50) van Koningsveld, H.; Koegler, J. H. *Microporous Mesoporous Mater.* **1997**, *9*, 71−81.

(51) Fischer, R. X.; W. H. Baur, W. H. *Zeolite-Type Crystal Structures and their Chemistry. Zeolite Structure Codes LTA to RHO.* ***Subvolume D*** in *Landolt-Börnstein, Numerical Data and Functional Relationships in Science and Technology, New Series, Group IV: Physical Chemistry, Volume **14**, Microporous and other Framework Materials with Zeolite-Type Structures*; Fischer, R. X., Baur, W. H., Eds.; Springer-Verlag: Berlin, 2006.

(52) van Koningsveld, H.; Jansen, J. C. *Microporous Mater.* **1966**, *6*, 159−167.

(53) Mentzen, B. F.; Sacerdote-Peronnet, M.; Bérar, J.-F.; Lefèbvre, F. *Zeolites* **1993**, *13*, 485−492.